High porewater exchange in a mangrove-dominated estuary revealed from short-lived radium isotopes

Mahmood Sadat-Noori[1,2*], Isaac R. Santos[1,2], Douglas R. Tait[1,2], Michael Reading[1], Christian J. Sanders[1]

[1]National Marine Science Centre, School of Environment, Science and Engineering, Southern Cross University, Coffs Harbour, NSW, Australia

[2]School of Environment, Science and Engineering, Southern Cross University, Lismore, NSW, Australia

[*]Corresponding author:

M. Sadat-Noori, School of Environment, Science and Engineering, Southern Cross University, PO Box 157 Lismore, NSW 2480, Australia (mahmood.sadat-noori@scu.edu.au)

Abstract

We hypothesise that mangroves play an important role in groundwater exchange processes in sub-tropical and tropical estuarine waters. To investigate this, multiple high resolution time series measurements of radium across a tidal estuary (Coffs Creek, NSW, Australia) were performed as well as a spatial survey in both bottom and surface layers. Results from the spatial survey revealed increasing radium concentrations in parts of the estuary surrounded by mangroves. The average radium concentration in estuary areas lined with mangroves was 2.5 times higher than the average concentration at the mouth of the estuary and 6.5-fold higher than upstream freshwater areas. Additionally, the area enriched in radium coincided with low dissolved oxygen concentrations, implying that porewater exchange may drive anoxia. A radium mass balance model based on ^{223}Ra and ^{224}Ra isotopes at different sections of the estuary confirmed higher porewater exchange rates from areas fringed with mangrove vegetation. Estimated porewater exchange rates were 27.8 ± 5.3 and 13.6 ± 2.1 cm d^{-1} (0.8 ± 0.1 and 0.4 ± 0.1 m^3 s^{-1}) based on ^{223}Ra and ^{224}Ra isotopes, respectively. The average saline porewater exchange was ~10-fold larger than the upstream surface freshwater inputs to the estuary. We suggest that mangrove environments within subtropical estuaries are hotspots for porewater exchange due to the complex belowground structure of crab burrows and the effect of tidal pumping. Because porewater exchange releases carbon and nitrogen from coastal sediments, development and modification of mangrove areas in subtropical estuaries can have a significant effect on coastal biogeochemical cycles.

Key Words: seepage, permeable sediments, submarine groundwater discharge, radon

1. Introduction

Submarine groundwater discharge (SGD) can include either or both the flow of fresh terrestrial groundwater and/or porewater exchange (saline recirculated seawater) into coastal waters. Where sediments are saturated, both the terms groundwater and porewater can be used to describe the water in below the sediment surface (Burnett et al., 2003). The origin of SGD can be from shallow and/or deep aquifers and the mechanisms driving SGD can include hydraulic gradient, tidal pumping, wave setup and density driven water convection occurring over various time and spatial scales (Santos et al., 2012a). The role of SGD is now recognized as a major component of water balances (Kwon et al., 2014; Sadat-Noori et al., 2016c), as a significant pathway for solute delivery to aquatic systems (Rodellas et al., 2015; Hong et al., 2017; Tait et al., 2017) and as a driver of biogeochemical processes in coastal environments (Moore, 2006). However, due to SGDs heterogeneous nature both in space and time, quantifying SGD remains a challenge (Burnett et al., 2006; Porubsky et al., 2014).

Natural geochemical tracers are now widely used to quantify SGD (Burnett et al., 2006; Trezzi et al., 2017). Radioactive nuclides such as radium isotopes (^{223}Ra, ^{224}Ra, ^{226}Ra and ^{228}Ra) have been used to quantify SGD rates in numerous aquatic systems including estuaries (Charette et al., 2013), lakes (Wang et al., 2016), rivers (Peterson et al., 2008), embayments (Stewart et al., 2015; Wang et al., 2016) and the continental shelf (Moore, 2000). Radium is a rare-earth metal produced from the decay of uranium/thorium and its concentration is often much higher in coastal groundwater relative to surface waters. The short-lived radium isotopes ^{223}Ra and ^{224}Ra have half-lives of 11.4 and 3.6 days which are on the same time scales of physical processes usually related to tidally-driven SGD and mixing in coastal waters (Burnett et al., 2008). Radium is attached to sediment particles and is released to solution when exposed to brackish or saline water due to ion exchange processes. This makes radium an ideal tool for quantifying recirculated seawater and saline groundwater (Moore, 2006). However, the labour-intensive nature of radium sampling often hinders the collection of large datasets.

Estuaries act as a pathway for solutes to enter the coastal ocean especially at times of high flow (Maher et al., 2015). Previous studies have shown that estuaries are significant sources of greenhouse gases, nutrients and dissolved carbon to the coastal ocean and have highlighted the important role SGD plays in this delivery process (Sadat-Noori et al., 2016a; Sadat-Noori et al., 2016b). SGD can also deliver low oxygen waters to coastal environments and cause hypoxia

(McCoy et al., 2011; Peterson et al., 2016). Low dissolved oxygen (DO) concentrations in the water column can disrupt key biogeochemical processes such as respiration and nitrification (Roberts et al., 2011). However, the role of SGD and porewater exchange processes in influencing hypoxia and anoxia conditions in coastal estuarine waters is still poorly understood.

Mangroves can play a significant role in biogeochemical processes in tropical coastal waters (Bouillon et al., 2008; Stieglitz et al., 2013; Tait et al., 2016). Mangroves can sequester carbon from the atmosphere, store large amounts of carbon belowground, provide a major pathway for carbon to travel from land to ocean and can facilitate nutrient cycling (Sanders et al., 2016; Sippo et al., 2016). This makes mangroves within estuarine ecosystems an important component of the global carbon cycle (Bouillon et al., 2008). Additionally, mangroves support many burrowing animal species (Nagelkerken et al., 2008). Burrows create large pore spaces in sediments that enhance the interaction between surface waters and porewater. Crab burrows can be extensive with previous studies suggesting that the subsurface area can be up to six times greater than the aboveground area (Stieglitz et al., 2000). Therefore, any alteration to mangrove habitat, including aquaculture expansion, coastal development and urbanization could alter SGD or porewater exchange rates and the release of dissolved carbon and nutrients to marine coastal waters.

SGD hotspots along rivers and estuaries can occur in areas with different vegetation, modifications and drainage settings. Sadat-Noori et al. (2015) used multiple radon (^{222}Rn) time series stations along the length of a subtropical tidal estuary to detect groundwater discharge rates at the mouth, mid-section and upstream parts of an estuary. The study showed a well-defined area of high groundwater discharge near sand dunes. Additionally, the study showed that multiple time series stations decreased the overall uncertainty of groundwater discharge estimates from 41% with one station to 23% with four by breaking down the estuary into smaller sections which reduces errors related to upscaling. Another way to further reduce uncertainties in mass balance models is through the use of radium. A radium mass balance model does not require estimating evasion rates which often have large uncertainties due to the use of empirical models used in evasion calculations. However, to date there has been no multiple radium isotope time series measurements in estuaries to quantify SGD rates from various sections within the estuary.

In this study, we hypothesize that estuarine areas surrounded by mangroves play an important role in groundwater exchange processes. Previous studies have used time series radium measurements to quantify SGD rates with a measuring station at the mouth of the estuary which

cannot reveal spatial distribution of SGD (Peterson et al., 2008a; Sadat-Noori et al., 2015; Tait et al., 2017). This study builds on the literature by combining multiple radium time series measurement stations along an estuarine gradient accompanied with a detailed spatial survey to quantify SGD rates and identify SGD hotspots. With our detailed sampling strategy, uncertainties can be reduced when estimating SGD rates.

2. Material and methods

2.1. Study site

The study was conducted at Coffs Creek estuary located at Coffs Harbour, NSW, Australia (33°17′48″S, 153°08′14″E) (Figure 1). Coffs Creek estuary is a tidal estuary, 6 km long, an average of 40 m wide and has an average depth of 0.6 m. The estuary's lower and central parts are surrounded by mangroves and saltmarsh vegetation with the highest densities in the mid estuary. Mangroves in Coffs Creek estuary cover an area of about 187,000 m^2. The estuary has a catchment area of about 25 km^2 of which 80% is dominated by urban development and agriculture, while just ~16% is considered undisturbed (Roper et al., 2011). The estuary accumulates sands in the first 4.5 km from the mouth of the estuary as a result of waves and storms. In the upper part of the estuary, silt and clay fractions increase. The region receives an average annual rainfall of 1600 mm, has a sub-tropical climate with hot and wet summers and cold and dry winters. The wettest and driest months are February and September, respectively. The water demand of Coffs Harbor is around 18 ML per day. Potable water for the city is pumped from the local rivers outside the catchment (Orara River, Nymboida River and Shannon Creek) and the wastewater from the city is treated before the effluent is disposed offshore (Coffs Harbor City Council, 2013).

A field campaign was conducted from the 1st to 7th March 2016. Although sampling was conducted in what is normally the wettest time of the year, El Niño conditions led to drier than normal conditions and thus lower than expected surface water flow in the estuary. The area did not receive any rainfall two weeks prior to the time series data collection. However, it received a total of 11.7 mm of rainfall during the sampling week with 7.2 mm on 4th March. Overall, no surface water runoff was observed during sampling from stormwater drains flowing into the estuary.

2.2. Radium time series measurements

For the time series experiment, radium samples were collected at five sites (A, B, C, D, E) along the length of the estuary over six consecutive days with the first site (Site A; 30°17'47.38"S, 153° 8'11.85"E) being located at the mouth of the estuary and the last site (Site E; 30°17'35.99"S, 153° 6'38.31"E) at the freshwater endpoint of the estuary (Figure 1). Sites B (30°17'30.97"S, 153° 7'25.97"E), C (30°17'41.17"S, 153° 7'5.40"E) and D (30°17'40.35"S, 153° 7'13.13"E) were located in between. For all sites (except E), radium samples were collected every 1 to 2 hours for at least 24 hours to capture two full tidal cycles and diurnal patterns. Site E samples were collected every 6 hours for 24 hours as it was not influenced by tides. To account for stratification in the water column between Sites C and D, radium samples for these sites were collected from the top and bottom layer of water column.

For each sample, estuary water was pumped from mid estuary into 100 L barrels which were drained through manganese-impregnated fibre at about 1 L min^{-1} with the fibres absorbing the dissolved radium from the water (Moore, 2010). The fibres were then transported to the laboratory within a day, rinsed with radium-free water to remove residual salt and particles, partially dried and placed in a Radium Delayed Coincide Counter (RaDeCC) for measuring ^{223}Ra and ^{224}Ra activities (Moore and Arnold, 1996) with analytical uncertainties calculated following Garcia-Solsona et al. (2008). Thereafter, samples were stored for a period of more than one month (>5 half-lives of ^{224}Ra) before being reanalysed through the RaDeCC to measure ^{228}Th activity to estimate the ^{224}Ra excess.

At each site, calibrated multi parameter sondes (Hydrolab DS5) measured temperature (˚C), DO (mg L^{-1}), pH and salinity every 15 minutes and depth loggers (Hobo CTD divers) measured estuary depth. An acoustic doppler current profiler (ADCP; Sontek Argonaut) was installed in the middle of the estuary at Site A to measure current velocity and direction of flow at 15 min intervals. Starflow ultrasonic Doppler flow meters were used at the four other sites to determine current velocity at the same intervals. Detailed depth profiles and cross sectional data of Coffs Creek estuary was acquired from the Office of Environment and Heritage, NSW government (www.environment.nsw.gov.au). Surface water discharge was calculated by multiplying current velocity by individual time specific cross sectional areas assuming that the currents across the channel were homogenous. Estuary water volume was estimated using an estuary area obtained from Google Earth imagery and the average depth of water from each site.

2.3. Radium survey measurements

A radium spatial survey was conducted on the 16th March 2016 to collect radium samples from the top and bottom layer of the estuary water column. A total of 10 locations along the estuary were sampled for temperature, DO, and salinity (YSI multiparameter probe) with measurements taken of the water column vertical profile every 20 cm from the bottom of the estuary. To determine radium concentrations, 20 L samples were collected from the bottom and top portions of the water column in the estuary. Radium samples were processed as described above. Survey maps were produced using the inverse distance weighted (IDW) interpolation method in GIS ArcMap 10 software.

2.4. Radium diffusion from sediments and desorption

Radium diffusion from sediments was measured by collecting five sediment core samples from each time series site. The sediment from the cores (approximately 5 L) were placed in a 20 L container and filled with radium free saline creek water comparable to bottom water salinities. For Site E, fresh water was used. Samples were incubated for two months (>5 half-lives of both ^{223}Ra and ^{224}Ra) when diffusion from sediments was assumed to be equivalent to decay losses in the overlying water. After this period, the overlaying water was extracted and drained through manganese impregnated fibre for ^{223}Ra and ^{224}Ra analysis. The decay flux of dissolved radium (i.e., radium inventory multiplied by decay constant) was assumed to equal diffusion.

To measure the potential radium desorption from suspended particles which are released due to ion exchange processes when influenced by brackish water, two 100 L barrels of fresh water (salinity ~ 0.1) were collected at the most upstream station. One barrel was used to quantify desorption, and another barrel was used to assess radium contamination in the salts used in the first barrel. In the first barrel, marine salt was added to increase salinity to the same salinity as Coffs Creek estuary's mouth (36). The water in the second barrel was filtered and drained through manganese fibre to create radium free water, and then pumped into another barrel. Salt was then added to the barrel to assess radium concentrations in the salt. The water in the barrels was stirred and left overnight for radium to be released from particles prior to drainage through manganese fibres. The difference between radium activity in the fresh water sample and the salted water was multiplied by estuary flow at the upstream station to estimate maximum potential fluxes of radium desorbed by suspended particles.

2.5. Groundwater sampling

A total of 14 groundwater samples were collected from four different locations along the estuarine salinity gradient near each time series site at low, mid and high tide marks (Figure 1). To sample groundwater, shallow bores ranging from 0.3 to 3.0 m deep were dug using a hand-held auger. PVC pipes with 50 cm long screens attached to the end were then installed and a peristaltic pump was used to purge the bore dry three times before water samples were collected. Ancillary data (temperature, DO and salinity) were obtained using a calibrated handheld multi-probe (YSI). For radium measurements, groundwater was collected in 6 L bottles which were filtered through manganese fibres at 1 L min^{-1} and analysed as above.

2.6. Radium mass balance model

To quantify porewater exchange, an integrated radium mass balance model was used which assumes steady state conditions over a 24-h sampling period (Peterson et al., 2010). To construct the model, the estuary was fragmented into four sections based on the time series site locations with each site being the boundary of a section. The sections are related to each other in terms of tracer fluxes by flood and ebb tides. For example, during flood tide the flux out of a downstream section acts as an input for the upstream section. Additionally, for calculating the porewater input from each section, the contribution of radium from adjoining sections was subtracted from the overall radium budget for that section. The model accounts for all the radium sources (upstream inputs, downstream tidal inputs, diffusion from bottom sediments, desorption from sediment particles and porewater exchange) and sinks (radium decay and downstream discharge) in the area between each site and assumes that groundwater/porewater is the missing term to balance the equation (Figure 2):

$$F_{GW}\,Ra_{GW} + Ra_{Diff}\,A\,h\,\lambda + Ra_{Desorp}\,D + Ra_{Upstream} = Ra\,V\,\lambda + Ra_{Net\ export} \quad (1)$$

where F_{GW} is the groundwater discharge ($m^3\ s^{-1}$), Ra_{GW} is the average groundwater endmember concentration (dpm m^{-3}), Ra_{Diff} is the diffusion from bottom sediments (dpm m^{-3}), A is estuary surface area (m^2), h is the average water depth in diffusion containers (m), λ is radium decay constant (0.0608 d^{-1} for ^{223}Ra and 0.1893 d^{-1} for ^{224}Ra), Ra_{Desorp} is desorption from suspended sediments (dpm m^{-3}), D is surface water discharge ($m^3\ s^{-1}$), $Ra_{Upstream}$ is the upstream Ra input flux

during flood tide (dpm s^{-1}), V is the weighted estuary water volume (m^3), and $Ra_{Net\ export}$ is the Ra downstream output net flux during ebb tides (dpm s^{-1}). A weighted estuary water volume was used to calculate radium decay across the estuary. At each spatial survey sampling point, the radium concentration from the top and bottom layer was separately multiplied by the water column depth and then by the area surrounding that specific point. The radium decay rate from the two layers were then added to obtain the final radium decay rate for the entire estuary. All fluxes were integrated over a 24-hr tidal cycle and the equation was solved for F_{GW}.

An uncertainty analysis was performed. Average radium concentration analytical uncertainties were 5 ± 1% with the highest uncertainty reaching 15% when radium activities were lowest. Readings from the current meter were assigned an uncertainty of 2% which was obtained from the manufacturer. To account for a maximum reasonable uncertainty, a total error of 10% was assigned for each of the calculated surface water discharge (flow) rates. An uncertainty of 5% was assigned to the average water depth in the diffusion container. The surface area and volume representing each measuring station was given a 10% error, while uncertainties in the groundwater endmember concentrations were assumed to be the natural variability. Uncertainties for each term in the mass balance were then calculated following standard propagation of error methods with analytical errors similar to Sadat-Noori et al. (2015).

Radium ages were calculated by a technique that compares activity ratios (AR) between a short and a longer-lived radium isotope where radium additions from sediments and groundwater are continuous (Moore, 2006). The method assumes that the system is in steady state and that radium additions through diffusion, desorption and groundwater to the system are balanced by losses. Radium water ages were calculated using the following equation (2) (Moore, 2006):

$$t = [F\ (^{224}Ra/^{223}Ra) - I\ (^{224}Ra\ /^{223}Ra)]/\ I\ (^{224}Ra\ /^{223}Ra)\ \lambda_{224} \quad (2)$$

where t indicates the apparent age of the water in the system; $F\ (^{224}Ra/^{223}Ra)$ is the activity ratio of the flux into the system; $I\ (^{224}Ra\ /^{223}Ra)$ is the observed activity ratio measured at the sampling point; and λ_{224} is the decay constants for ^{224}Ra isotopes.

3. Results

253 3.1. Surface water time series

254 At the mouth of the estuary, salinity followed a tidal trend with higher values at high tide and
255 lower values at low tide however, they remained higher than 35 during both high and low tide.
256 Dissolved oxygen also showed a tidal cycle that reached a maximum of 111% at high tide and
257 dropped to 65% at low tide (Figure 3). Salinity at Site B varied between 27 to 34 with an average
258 of 32 ± 0.3. DO at Site B was lower than Site A with an average of 36 ± 1.1% saturation. Salinity
259 at Site C and D was only slightly affected by tidal cycles and had an average salinity of 26 ± 0.5
260 and 19 ± 0.5, respectively. However, at Site D, salinity in the top layer averaged 9.5 ± 0.5 while
261 in the bottom layer it was much higher with an average of 29 ± 0.5.

262 Site A radium concentrations followed an inverse tidal trend and were clearly seen to have the
263 highest values at lower water levels (low tide) (Figure 3). Average ^{223}Ra and ^{224}Ra concentrations
264 at Site A were 5.1 ± 0.3 and 80.6 ± 1.3 dpm 100 L^{-1} (all uncertainties in concentrations refer to
265 standard error). The average ^{223}Ra concentration at Site B (13.8 ± 08 dpm 100 L^{-1}) was 2.7, 2 and
266 3-fold higher than Site A, C and D, respectively. The same trend was observed in ^{224}Ra
267 concentrations with the lowest concentration observed at the freshwater Site E. The top and bottom
268 layers at site C had average ^{223}Ra concentrations of 6.2 ± 0.2 and 9.2 ± 0.8 dpm 100 L^{-1} and ^{224}Ra
269 concentrations of 60.2 ± 1.9 and 93.7 ± 2.3 dpm 100L^{-1} respectively. At Site D, the top and bottom
270 layer average ^{223}Ra concentrations were lower than Sites A, B and C and were 3.6 ± 0.4 and 5.0 ±
271 0.4 dpm 100 L^{-1} and ^{224}Ra concentrations were 44.9 ± 1.5 and 62.6 ± 1.6 dpm 100L^{-1}. There were
272 no clear tidal trends for radium at Sites B, C, D and E.

273 3.2. Surface water survey

274 Salinity depth profiles showed that there was a saline bottom layer up to 5 km (between survey
275 stations 8 and 9) from the mouth of the estuary and a brackish water top layer up to 3 km from the
276 mouth (Station 4). There was high dissolved oxygen content in the water column up to 3 km from
277 the mouth of the estuary and a depletion of dissolved oxygen in the upper parts of the estuary from
278 20 cm below the surface to the creek bed (Figure 4). Temperatures were higher in the mid-section
279 of the estuary compared to the mouth and upstream. Higher ^{223}Ra and ^{224}Ra concentrations were
280 observed in middle parts of the estuary (Station 5) while lower concentrations of both radium
281 isotopes were seen upstream (Station 10) and at the mouth of the estuary (Station 1) in both top

and bottom layers (Figure 5). The highest radium concentrations occurred in areas of the estuary were most mangroves and brackish waters were present.

3.3 Groundwater

Salinity in groundwater samples ranged from fresh (0.2) to saline (32.1) with an average of 19.8 ± 2.9. Dissolved oxygen saturation in the groundwater varied from almost zero (0.6%) to 83% with most samples having less than 50% saturation. The average groundwater ^{223}Ra and ^{224}Ra concentrations were 33.5 ± 7.1 and 1046.6 ± 177.6 dpm 100 L^{-1} respectively, and were approximately 5.5 and 15-fold higher than average surface water observations from all the sites (Table 1).

3.4. Radium diffusion and desorption from suspended sediments

The average diffusion rates for the entire estuary were very low at 0.9 ± 0.2 dpm m^{-2} day^{-1} for ^{223}Ra and 44.7 ± 2.0 dpm m^{-2} day^{-1} for ^{224}Ra. Diffusive rates from adjacent sites (i.e. Site A and B) were used to extrapolate diffusion fluxes based on the area between sites. Estimated diffusive fluxes from the sediment incubation experiment were highest for the area between Site A – B (2.5 ± 0.5 and 39.4 ± 1.7 dpm s^{-1} for ^{223}Ra and ^{224}Ra, respectively), but still accounted for less than 1% of downstream exports. Diffusion from other sections were less than 10% of those observed for the area between Site A – B.

Average desorption rates from suspended sediments were also negligible with rates of 2.1 ± 1.0 dpm s^{-1} for ^{223}Ra and 21.7 ± 2.7 dpm s^{-1} for ^{224}Ra, respectively. These fluxes were assumed to occur only near the most upstream station where fresh river water first meets brackish estuarine waters. Desorption from suspended sediments and decay were less than 7% of the total radium losses at the most downstream estuary station and were minor components of the mass balance model for both radium isotopes for all sections (Table 2).

3.5. Radium mass balance

The radium mass balance model was overwhelmingly dominated by downstream net outputs (i.e., tidal exchange with the ocean; Table 2) in each section. Using both ^{223}Ra and ^{224}Ra, the highest volumetric porewater input was from the area between Site A – B (0.7 ± 0.1 and 0.3 ± 0.1 m^3 s^{-1}, respectively). However, based on per unit area the highest input of porewater was from the

area between Site B – C (31.3 ± 5.9 cm d^{-1} for ^{223}Ra and 22.0 ± 2.5 cm d^{-1} for ^{224}Ra) followed by A – B (28.0 ± 6.1 and 13.5± 2.3 cm d^{-1} for ^{223}Ra and ^{224}Ra, respectively) which was surrounded by mangroves. The lowest porewater input was from the area between Site C – D which had no mangroves (Figure 6). Using the average groundwater endmember concentrations, total (i.e. sum of all sections) volumetric porewater exchange rates of 0.8 ± 0.1 and 0.4 ± 0.1 m^3 s^{-1} were calculated for ^{223}Ra and ^{224}Ra respectively. Based on the total estuary area of 237,538 m^2, total estuarine porewater exchange fluxes were estimated to be 27.8 ± 5.3 and 13.6 ± 2.1 cm d^{-1} using ^{223}Ra and ^{224}Ra respectively (Table 2). Uncertainties for porewater exchange rates were 19 and 15% for ^{223}Ra and ^{224}Ra, respectively.

4. Discussion

Radium concentrations increased in the mid-section of the estuary where brackish water and mangroves were present (Figure 5). Additionally, salinity scatter plots indicated a non-conservative behaviour for both radium isotopes with more enrichment in brackish and saline water (Figure 7) that cannot be explained by upstream freshwater inputs, desorption nor diffusion. The only reasonable source of radium is enhanced porewater exchange in that section of the estuary. Previous studies have shown that mangroves can play a significant role in porewater exchange processes and often have large porewater exchange rates (Gleeson et al., 2013; Stieglitz et al., 2005; Tait et al., 2017). Stieglitz et al. (2013) showed that burrow flushing in mangroves can deliver high concentrations of ^{222}Rn and radium isotopes to surface waters in Hinchinbrook Island, Australia. In a latitudinal study across Australia, Tait et al. (2016) showed that mangrove sites have larger porewater exchange rates than sites with other vegetation such as salt marsh. Porewater fluxes calculated via the mass balance also offer strong evidence that porewater exchange increases in the mangrove dominated sections of the estuary. Higher porewater input rates were aligned with areas fringed with mangrove vegetation and sections that had a higher ratio of mangrove area to estuary area corresponded to higher porewater exchange rates (Figure 6). Although mangrove sediments often have low permeability, large pore spaces such as crab burrows are thought to intensify porewater exchange rates (Stieglitz et al., 2000). Therefore, the mangrove environment in the mid-section of the estuary likely drives high porewater exchange rates which elevates surface water radium concentrations.

Multiple radium time series stations revealed that porewater exchange occurred at different rates along the length of the estuary. For example, here we found the highest porewater exchange to occur in the mid-section of the estuary (Site B - C) and the lowest exchange rate just upstream between Sites C and D. A single time series measuring station at the mouth of an estuary can capture temporal variability in radium concentrations. However, this approach may not fully capture spatial variations occurring along the length of the estuary (Peterson et al., 2008a; Sadat-Noori et al., 2015). Therefore, a multiple time series measurement station strategy can better constrain tracer variations in estuarine environments with different settings between its boundaries. Similar to other tidal systems (Garcia-Orellana et al., 2010; Tait et al., 2017), tidal inputs and outputs of radium were at least an order of magnitude higher than any other term in the mass balance in all sections. This high contribution of tidal net export may hinder the construction of a mass balance using only a spatial survey approach, further highlighting the importance of time series measurements in quantifying porewater exchange in tidal estuaries with high temporal variability. Here, if we had only used one station at the mouth of the estuary, the average total porewater exchange rate (0.6 ± 0.1 m^3 s^{-1}) would have not changed volumetrically due to the dominant effect of tidal downstream outputs at the mouth of the estuary. However, by using only a single station, a quantitative detection of higher groundwater inputs in the mid-section of the estuary would not have been possible. In contrast, other studies using multiple radon measuring stations found upstream inputs important and reported the highest groundwater/porewater rates were from the most upstream areas of the estuary (Sadat-Noori et al., 2015).

Our estimates fall within other studies quantifying porewater exchange in tidal estuaries with mangrove vegetation. Gleeson et al. (2013) used a single radium time series station combined with a Eularian approach at the mouth of a mangrove dominated tidal estuary in Southern Moreton Bay, QLD, Australia, and reported an average porewater exchange rate of 17 cm d^{-1}, similar to the average ^{223}Ra and ^{224}Ra porewater exchange rates calculated here (20.7 ± 3.6 cm d^{-1}). In another study, average porewater exchange rates via a single radium measuring station in a sub-tropical tidal estuary with similar mid-section mangrove areas to Coffs Creek estuary was 19 ± 6 cm d^{-1} (Sadat-Noori et al., 2015).

Endmember concentrations in groundwater are often considered the most significant source of uncertainty in using natural tracer mass balance techniques (Dulaiova et al., 2008; Cho and Kim, 2016). Most previous studies have used the average radium groundwater concentration as the

groundwater endmember (Kwon et al., 2014; Lee et al., 2012; Sadat-Noori et al., 2015; Tait et al., 2017) while some have considered the maximum radium concentration to avoid overestimation (Moore, 1996; Stewart et al., 2015). If we use the maximum groundwater ^{223}Ra (113.80 dpm 100 L^{-1}) and ^{224}Ra (2557.3 dpm 100 L^{-1}) activities, total porewater exchange rates would decrease from those calculated using the average groundwater radium concentration by 70 and 90% for ^{223}Ra and ^{224}Ra, respectively. If we assume the relatively fresh groundwater samples do not represent the endmember concentration and use only groundwater samples with a salinity >20 as endmembers, similar porewater exchange rates to the maximum scenario would be estimated. If the section specific average groundwater radium endmembers were used, similar total porewater exchange rates for both radium isotopes would be estimated. Here, we opted to use the average groundwater endmember as our sampling locations (Figure 1, blue dots) covered the entire estuary length and the sample size (n = 14) is reasonable.

Another source of uncertainty around porewater exchange estimates is due to the sampling at the five stations taking place over multiple days rather than simultaneously. Previous studies in mangrove systems have reported that larger tidal ranges drive greater tidal pumping which can influence porewater exchange rates (Tait et al., 2016). Here, despite sampling over multiple days, little difference was observed between the maximum tidal range at each site (0.58 – 0.61 m) (Figure 3) and there was little change in atmospheric conditions and minimal rainfall over the course of the study. Therefore, we assume that similar rates of porewater exchange occurred over the course of sampling at each site. While logistically challenging, performing time series measurements simultaneously at all sites could further reduce uncertainties around porewater exchange estimates.

In most previous studies, porewater exchange rates estimated from short-lived radium isotopes (^{223}Ra and ^{224}Ra) are within a close range (Rodellas et al., 2017; Sadat-Noori et al., 2016; Gleeson, et al., 2013). Here, porewater exchange rates estimated based on ^{223}Ra were approximately twice as high than estimates using ^{224}Ra (Table 2). This is unlikely to be associated with different geochemical behaviour of isotopes as both isotopes react similarly and reach sorption equilibrium rapidly (Gonneea et al., 2008; Luek and Beck, et al., 2015). A ^{223}Ra vs ^{224}Ra activity ratio plot showed a very close correlation indicating similar sources for both isotopes (Figure 8). The differences could be due to the different half-lives associated with each of the isotopes used as groundwater endmembers. While ^{223}Ra regenerates on time scales of weeks due to its 11.4 day half-life, ^{224}Ra (half-life 3.6 days) regenerates in sediments on shorter time scales, probably

explaining the relative enrichment of ^{224}Ra in porewater. Previous studies have also suggested that different quantities of radium isotopes can be suppled as a function of their half-lives (Luek and Beck, et al., 2015; Bollinger and Moore, 1993).

To investigate this further, we used ^{223}Ra and ^{224}Ra isotopes to establish the apparent radium water age within Coffs Creek estuary. Previous studies have also used the short-lived radium isotopes ^{223}Ra and ^{224}Ra to estimate radium water ages and residence time in estuarine coastal waters (Dulaiova and Burnett, 2008; Moore, 2000; Peterson et al., 2008b). Here, the average radium age for the entire estuary was seven days while in the mid-section (area between Sites B - C) the average radium age was nine days (Figure 5). This implies that in this section of the estuary, the ^{224}Ra from porewater had already decayed more than two half-lives while the ^{223}Ra had only decayed less than one of its half-life. This could explain the lower calculated porewater fluxes from ^{224}Ra isotope. Previous studies have also found higher porewater exchange rates estimated using ^{224}Ra isotopes compared to ^{223}Ra isotopes in a series of mangrove estuaries on the east coast of Australia (Tait et al., 2017).

The total average flux calculated based on ^{223}Ra and ^{224}Ra indicated that porewater exchange was equivalent to 11- to 25-fold of the discharging fresh surface water out of the estuary. A groundwater discharge of this magnitude is not uncommon with previous studies in a tidal river with typical salt-wedge estuarine circulation (Indian River Lagoon, USA) reporting groundwater accounting for up to 80% of surface water discharge (Peterson et al., 2010). In another study in a subtropical Australian estuary, groundwater discharge was shown to be responsible for 79% of the downstream water flow (Atkins et al., 2013). Here, the majority of groundwater is assumed to be saline rather than fresh as radium mainly represents saline recirculated seawater rather than fresh groundwater (Mulligan and Charette, 2006), and the mid estuary mangroves favour tidally driven recirculation in sediments (Stieglitz et al., 2013; Gleeson et al., 2013; Tait et al., 2016). In this estuary, water likely infiltrates into the estuary banks at high tide, passes through the extensive crab burrows in the mangrove sediments and is released to the estuary as the tide drops. The higher radium concentrations in surface water at low tide (Figure 3) supports this hypothesis. A hysteresis pattern was evident from a radium versus water depth plot (Figure 9). During flood tide radium concentrations are low due to dilution. As the tide starts to drop, recirculated estuary water which has picked up a radium signal from the sediments enters the estuary, increasing radium concentrations. As the tide changes back to flood, low radium concentration seawater suddenly

enters the estuary while the water depth remains relatively unchanged. This supports the idea that tidal pumping in mangrove sediments was the main mechanism driving porewater exchange in the estuary, rather than processes such as molecular diffusion and bioturbation which are considered to be only minor contributors. Bioirrigation is also expected to release radium isotopes, but this is unlikely in Coffs Creek estuary because the areas with higher radium concentration were usually low in dissolved oxygen which prevents significant fauna activity (Santos et al., 2012b).

The freshwater discharge calculated via the freshwater fraction exported to the ocean also supports the notion of tidal pumping being the dominant process driving high porewater exchange rates. By using salinity and discharges at the mouth of the estuary integrated over 24 h (two complete tides), we estimate only 0.1 m^3 s^{-1} of fresh surface water discharge out of the estuary. The minor difference between freshwater fluxes at the upstream site (Sites E; 0.08 m^3 s^{-1}) and freshwater discharge at the mouth (Site A) can be assumed to represent fresh SGD (0.02 m^3 s^{-1}) along the length of the estuary because no lateral surface freshwater flows were observed. A comparison between fresh SGD estimated from the freshwater fraction with saline porewater exchange (0.6 ± 0.1 m^3 s^{-1}) estimated from the radium mass balance indicates that more than 90% of the discharging groundwater was saline. In comparison, Santos et al., (2015) reported recirculated seawater accounted for about 51% of the estimated total volume of porewater exchange in Waikareao Estuary, New Zealand. In another study, a similar approach was applied in a tidal estuary where dry season recirculated seawater was reported to account for 80% of the total groundwater/porewater exchange into the estuary (Sadat-Noori et al., 2015).

Previous studies have shown hypoxia conditions can be driven by groundwater discharge to bottom waters with high radium concentrations and low DO (<60% saturation) (Peterson et al., 2016). In this study, the estuary was stratified with a fresher top layer from the mid-section to the upstream extent overlying a more saline bottom layer (Figure 10). The results from the spatial survey revealed radium hotspot areas coincide with low DO areas predominantly in bottom saline waters (Figure 5). Additionally, a radium versus salinity scatter plot showed that radium activities in the mangrove dominated mid-section of the estuary are higher in bottom waters and coincide with low DO values with <30% saturation (Figures 7 and 10). Groundwater samples were mainly depleted in oxygen and enriched in radium. Since radium diffusion from bottom sediments (which can also increase radium activities in the bottom layer) was negligible, we speculate that anoxic groundwater inputs can be partially responsible for oxygen deficit in bottom waters. However,

detailed investigations of all sources and sinks of dissolved oxygen would be required to test these hypotheses for Coffs Creek estuary.

5. Conclusions

We combined multiple radium time series and spatial survey sampling in an estuarine environment. The spatial survey (top and bottom layer) and five times series stations along the gradient of the estuary helped estimate porewater exchange rates for different sections of the estuary and provided insight on the groundwater discharge locations. A ^{223}Ra and ^{224}Ra mass balance model provided quantitative evidence that considerable amounts of saline porewater was recirculating in sediments from a mangrove dominated section of the estuary. We suggest mangroves play a major role in subtropical estuaries to distinctively increase porewater exchange rates. This higher exchange can potentially release nutrients, dissolved carbon and greenhouse gases from sediments.

Acknowledgments

We would like to thank Dr. Damien Maher for his valuable comments and constructive suggestions that strengthened the manuscript. We would also like to thank Luke Jeffrey, Corinna Mori, Summer Barron and Jackie Webb for their contribution with data collection and to Ceylena Holloway for her outstanding logistical support during field and laboratory investigations. This research was partially funded through the Australian Research Council (DE140101733, DP150103286 and LE140100083) and the Herman Slade Foundation.

References

Atkins, M.L., Santos, I.R., Ruiz-Halpern, S. and Maher, D.T., 2013. Carbon dioxide dynamics driven by groundwater discharge in a coastal floodplain creek. Journal of Hydrology, 493, 30-42.

Bollinger, M.S. and Moore, W.S., 1993. Evaluation of salt marsh hydrology using radium as a tracer. Geochimica et Cosmochimica Acta, 57(10), 2203-2212.

Bouillon, S., Borges, A.V., Castañeda-Moya, E., Diele, K., Dittmar, T., Duke, N.C., Kristensen, E., Lee, S.Y., Marchand, C., Middelburg, J.J. and Rivera-Monroy, V.H., 2008. Mangrove production and carbon sinks: a revision of global budget estimates. Global Biogeochemical Cycles, 22(2).

Burnett, W.C., Aggarwal, P.K., Aureli, A., Bokuniewicz, H., Cable, J.E., Charette, M.A., Kontar, E., Krupa, S., Kulkarni, K.M., Loveless, A. and Moore, W.S., 2006. Quantifying

submarine groundwater discharge in the coastal zone via multiple methods. Science of the Total Environment, 367(2), 498-543.

Burnett, W.C., Bokuniewicz, H., Huettel, M., Moore, W.S. and Taniguchi, M., 2003. Groundwater and pore water inputs to the coastal zone. Biogeochemistry, 66(1-2), 3-33.

Burnett, W.C., Peterson, R., Moore, W.S., and de Oliveira, J., 2008. Radon and radium isotopes as tracers of submarine groundwater discharge-results from the Ubatuba, Brazil SGD assessment intercomparison. Estuarine, Coastal and Shelf Science, 76, 501–511.

Charette, M.A., and Allen, M.C., 2006. Precision Ground Water Sampling in Coastal Aquifers Using a Direct-Push, Shielded-Screen Well-Point System. Groundwater Monitoring and Remediation, 528 26, 87-93.

Charette, M.A., Henderson, P.B., Breier, C.F., and Liu, Q., 2013. Submarine groundwater discharge in a river-dominated Florida estuary. Marine Chemistry, 156, 3-17.

Cho, H.-M., and Kim, G., 2016. Determining groundwater Ra endmember values for the estimation of the magnitude of submarine groundwater discharge using Ra isotope tracers. Geophysical Research Letters, 43, 3865–3871, doi:10.1002/2016GL068805.

Coffs Harbour City Council, 2013. Coffs Creek Estuary Coastal Zone Management Plan - Estuary Condition Study, Coffs Harbour: Geolink Environmental Management and Design.

Dulaiova, H. and Burnett, W.C., 2008. Evaluation of the flushing rates of Apalachicola Bay, Florida via natural geochemical tracers. Marine Chemistry, 109(3), 395-408.

Garcia-Orellana, J., Cochran, J.K., Bokuniewicz, H., Yang, S., and Beck, A.J., 2010. Time series sampling of ^{223}Ra and ^{224}Ra at the inlet to Great South Bay (New York): a strategy for characterizing the dominant terms in the Ra budget of the bay. Journal of Environmental Radioactivity, 10, 582-588.

Garcia-Solsona, E., Garcia-Orellana, J., Masque, P., and Dulaiova, H., 2008. Uncertainties associated with ^{223}Ra and ^{224}Ra measurements in water via a Delayed Coincidence Counter (RaDeCC). Marine Chemistry, 109, 198–219.

Gleeson, J., Santos I.R., Maher D.T., and Golsby-Smith, L., 2013. Groundwater-surface water exchange in a mangrove tidal creek: Evidence from natural geochemical tracers and implications for nutrient budgets. Marine Chemistry, 156, 27–37.

Gonneea, M.E., Morris, P.J., Dulaiova, H. and Charette, M.A., 2008. New perspectives on radium behavior within a subterranean estuary. Marine Chemistry, 109(3), 250-267.

Hong, Q., Cai, P., Shi, X., Li, Q. and Wang, G., 2017. Solute transport into the Jiulong River estuary via porewater exchange and submarine groundwater discharge: New insights from 224 Ra/228 Th disequilibrium. Geochimica et Cosmochimica Acta, 198, 338-359.

Jeffrey, L.C., Maher, D.T., Santos, I.R., McMahon, A. and Tait, D.R., 2016. Groundwater, acid and carbon dioxide dynamics along a coastal wetland, lake and estuary continuum. Estuaries and Coasts, 39(5), 1325-1344.

Kwon, E.Y., Kim, G., Primeau, F., Moore, W.S., Cho, H.M., DeVries, T., Sarmiento, J.L., Charette, M.A., and Cho, Y.K., 2014. Global estimate of submarine groundwater

discharge based on an observationally constrained radium isotope model. Geophysical Research Letters, 41, 23, 8438–8444,

Lee, C.M., Jiao, J.J., Luo X., and Moore, W.S., 2012. Estimation of submarine groundwater discharge and associated nutrient fluxes in Tolo Harbour, Hong Kong. Science of the Total Environment, 433, 427–433.

Luek, J.L. and Beck, A.J., 2014. Radium budget of the York River estuary (VA, USA) dominated by submarine groundwater discharge with a seasonally variable groundwater end-member. Marine Chemistry, 165, 55-65.

Maher, D.T., Cowley, K., Santos, I.R., Macklin, P. and Eyre, B.D., 2015. Methane and carbon dioxide dynamics in a subtropical estuary over a diel cycle: Insights from automated in situ radioactive and stable isotope measurements. Marine Chemistry, 168, 69-79.

McCoy, C., Viso, R., Peterson, R.N., Libes, S., Lewis, B., Ledoux, J., Voulgaris, G., Smith, E. and Sanger, D., 2011. Radon as an indicator of limited cross-shelf mixing of submarine groundwater discharge along an open ocean beach in the South Atlantic Bight during observed hypoxia. Continental Shelf Research, 31(12), 1306-1317.

Moore, W.S., 2000. Ages of continental shelf waters determined from ^{223}Ra and ^{224}Ra. Journal of Geophysical Research, 105 (C9),117–122.

Moore, W.S., 2006. Radium isotopes as tracers of submarine groundwater discharge in Sicily. Continental Shelf Research, 26 (7), 852–861.

Moore, W.S., 2006. The role of submarine groundwater discharge in coastal biogeochemistry. Journal of Geochemical Exploration, 88(1), 389-393.

Moore, W.S., 2010. The effect of submarine groundwater discharge on the ocean. Annual Review of Marine Sciences, 2, 59–88.

Moore, W.S., Arnold, R., 1996. Measurement of ^{223}Ra and ^{224}Ra in coastal waters using a delayed coincidence counter. Journal of Geophysical Research, 101, 1321–1329.

Moore, W.S., Blanton, J.O. and Joye, S.B., 2006. Estimates of flushing times, submarine groundwater discharge, and nutrient fluxes to Okatee Estuary, South Carolina. Journal of Geophysical Research: Oceans, 111(C9).

Mulligan, A.E., Charette, M.A., 2006. Intercomparison of submarine groundwater discharge estimates from a sandy unconfined aquifer. Journal of Hydrology, 327, 411–425.

Nagelkerken, I.S.J.M., Blaber, S.J.M., Bouillon, S., Green, P., Haywood, M., Kirton, L.G., Meynecke, J.O., Pawlik, J., Penrose, H.M., Sasekumar, A. and Somerfield, P.J., 2008. The habitat function of mangroves for terrestrial and marine fauna: a review. Aquatic Botany, 89(2), 155-185.

Peterson, R.N., Burnett, W.C., Taniguchi, M., Chen, J., Santos, I.R., and Ishitobi, T., 2008a. Radon and radium isotope assessment of submarine groundwater discharge in the Yellow River delta, China. Journal of Geophysical Research, 113, 9–21.

Peterson, R.N., Burnett, W.C., Taniguchi, M., Chen, J., Santos, I.R. and Misra, S., 2008b. Determination of transport rates in the Yellow River–Bohai Sea mixing zone via natural geochemical tracers. Continental Shelf Research, 28(19), 2700-2707.

575 Peterson, R.N., Moore, W.S., Chappel, S.L., Viso, R.F., Libes, S.M. and Peterson, L.E., 2016. A
576 new perspective on coastal hypoxia: the role of saline groundwater. Marine
577 Chemistry, 179, 1-11.
578 Peterson, R.N., Santos, I.R., Burnett, W.C., 2010. Evaluating groundwater discharge to tidal rivers
579 based on a Rn-222 time-series approach. Estuarine, Coast and Shelf Science. 86, 165–
580 178.
581 Porubsky, W.P., Weston, N.B., Mooreb, W.S., Ruppel, C., and Joye, S.B., 2014. Dynamics of
582 submarine groundwater discharge and associated fluxes of dissolved nutrients, carbon,
583 and trace gases to the coastal zone (Okatee River estuary, South Carolina). Geochimca et
584 Cosmochimca Acta. 131, 81–97.
585 Roberts, K.L., Eate, V.M., Eyre, B.D., Holland, D. and Cook, P.L.M. 2012. Hypoxic events
586 stimulate nitrogen recycling in a shallow salt wedge estuary: the Yarra River Estuary,
587 Australian. Limnology and Oceanography 57, 1427-1442.
588 Rodellas, V., Garcia-Orellana, J., Masqué, P., Feldman, M. and Weinstein, Y., 2015. Submarine
589 groundwater discharge as a major source of nutrients to the Mediterranean
590 Sea. Proceedings of the National Academy of Sciences, 112(13), 3926-3930.
591 Roper, T., Creese, B., Scanes, P., Stephens, K., Williams, R., Dela-Cruz, J., Coade, G., Coates, B.
592 and Fraser, M., 2011. Assessing the condition of estuaries and coastal lake ecosystems in
593 NSW, Monitoring, evaluation and reporting program, Technical report series. Office of
594 Environment and Heritage, Sydney.
595 Sadat-Noori, M., Maher, D.T. and Santos, I.R., 2016a. Groundwater discharge as a source of
596 dissolved carbon and greenhouse gases in a subtropical estuary. Estuaries and
597 Coasts, 39(3), 639-656.
598 Sadat-Noori, M., Santos, I.R., Sanders, C.J., Sanders, L.M. and Maher, D.T., 2015. Groundwater
599 discharge into an estuary using spatially distributed radon time series and radium
600 isotopes. Journal of Hydrology, 528, 703-719.
601 Sadat-Noori, M., Santos, I.R., Tait, D.R. and Maher, D.T., 2016b. Fresh meteoric versus
602 recirculated saline groundwater nutrient inputs into a subtropical estuary. Science of the
603 Total Environment, 566, 1440-1453.
604 Sadat-Noori, M., Santos, I.R., Tait, D.R., McMahon, A., Kadel, S. and Maher, D.T., 2016c.
605 Intermittently Closed and Open Lakes and/or Lagoons (ICOLLs) as groundwater-
606 dominated coastal systems: Evidence from seasonal radon observations. Journal of
607 Hydrology, 535, 612-624.
608 Sanders, C.J., Maher, D.T., Tait, D.R., Williams, D., Holloway, C., Sippo, J.Z., and Santos, I.R.,
609 2016. Are global mangrove carbon stocks driven by rainfall? Journal of Geophysical
610 Research: Biogeosciences 121, 2600-2609.
611 Santos, I.R. and Eyre, B.D., 2011. Radon tracing of groundwater discharge into an Australian
612 estuary surrounded by coastal acid sulphate soils. Journal of Hydrology, 396(3), 246-257.

Santos, I.R., Cook, P.L., Rogers, L., Weys, J.D. and Eyre, B.D., 2012b. The "salt wedge pump": Convection-driven pore-water exchange as a source of dissolved organic and inorganic carbon and nitrogen to an estuary. Limnology and Oceanography, 57(5), 1415-1426.

Santos, I.R., Eyre, B.D. and Huettel, M., 2012a. The driving forces of porewater and groundwater flow in permeable coastal sediments: A review. Estuarine, Coastal and Shelf Science, 98, 1-15.

Sippo, J.Z., Maher, D.T., Tait, D.R., Ruiz-Halpern, S., Sanders, C.J. and Santos, I.R., 2017. Mangrove outwelling is a significant source of oceanic exchangeable organic carbon. Limnology and Oceanography Letters, 2(1),1-8.

Stewart, B.T., Santos, I.R., Tait, D.R., Macklin, P.A., and Maher, D.T., 2015. Submarine groundwater discharge and associated fluxes of alkalinity and dissolved carbon into Moreton Bay (Australia) estimated via radium isotopes. Marine Chemistry 174, 1-12.

Stieglitz, T.C., Clark, J.F., and Hancock, G.J., 2013. The mangrove pump: The tidal flushing of animal burrows in a tropical mangrove forest determined from radionuclide budgets. Geochimica et Cosmochimica Acta, 102, 12–22.

Stieglitz, T., 2005. Submarine groundwater discharge into the near-shore zone of the Great Barrier Reef, Australia. Marine Pollution Billiton, 51 (1–4), 51–59.

Stieglitz, T.C., Ridd, P., Müller, P., 2000. Passive irrigation and functional morphology of crustacean burrows in a tropical mangrove swamp. Hydrobiologia 421, 69-76.

Tait, D.R., Maher, D.T., Macklin, P.A. and Santos, I.R., 2016. Mangrove porewater exchange across a latitudinal gradient. Geophysical Research Letters, 43(7), 3334-3341.

Tait, D.R., Maher, D.T., Sanders, C.J. and Santos, I.R., 2017. Radium-derived porewater exchange and dissolved N and P fluxes in mangroves. Geochimica et Cosmochimica Acta. 200, 295–309.

Trezzi, G., Garcia-Orellana, J., Rodellas, V., Masqué, P., Garcia-Solsona, E. and Andersson, P.S., 2017. Assessing the role of submarine groundwater discharge as a source of Sr to the Mediterranean Sea. Geochimica et Cosmochimica Acta, 200, 42-54.

Wang, X. and Du, J., 2016. Submarine groundwater discharge into typical tropical lagoons: A case study in eastern Hainan Island, China. Geochemistry, Geophysics, Geosystems, 17(11), 4366-4382.

Wang, X., Li, H., Luo, X., Jiao, J., Qu, W. and Wang, C., 2016. Using 224Ra to estimate eddy diffusivity and submarine groundwater discharge in Laizhou Bay, China. Journal of Radioanalytical and Nuclear Chemistry, 308(2), 403-411.

Figure 1. Map of the Coffs Creek estuary, Australia. Site A to E indicate time series data collection locations. Grey boxes (labelled 1 to 10) indicate radium spatial survey sampling locations. Mangrove vegetation areas are highlighted in light green.

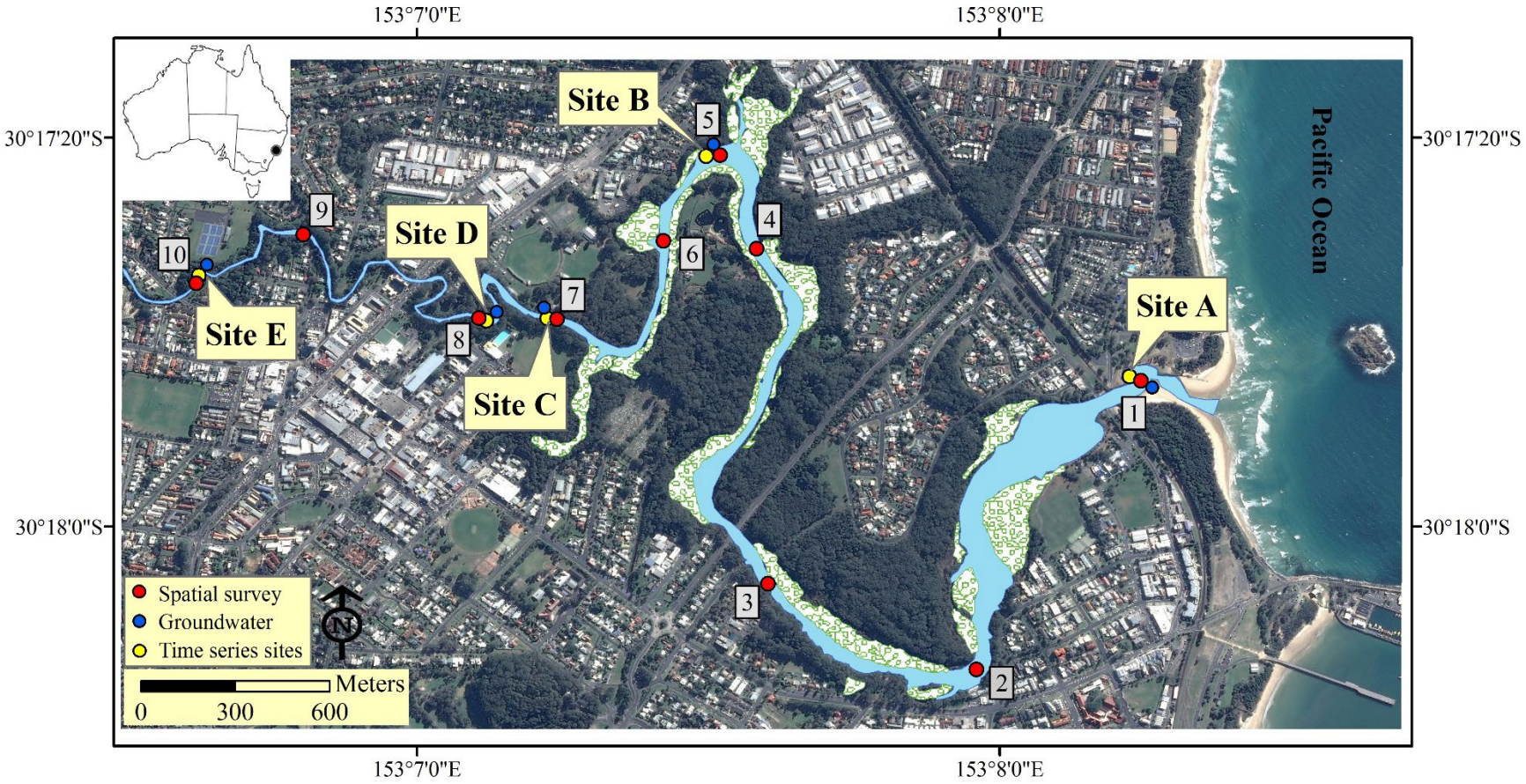

652 Figure 2. Conceptual model illustrating radium sources (blue arrows) and sinks (yellow arrows).

653

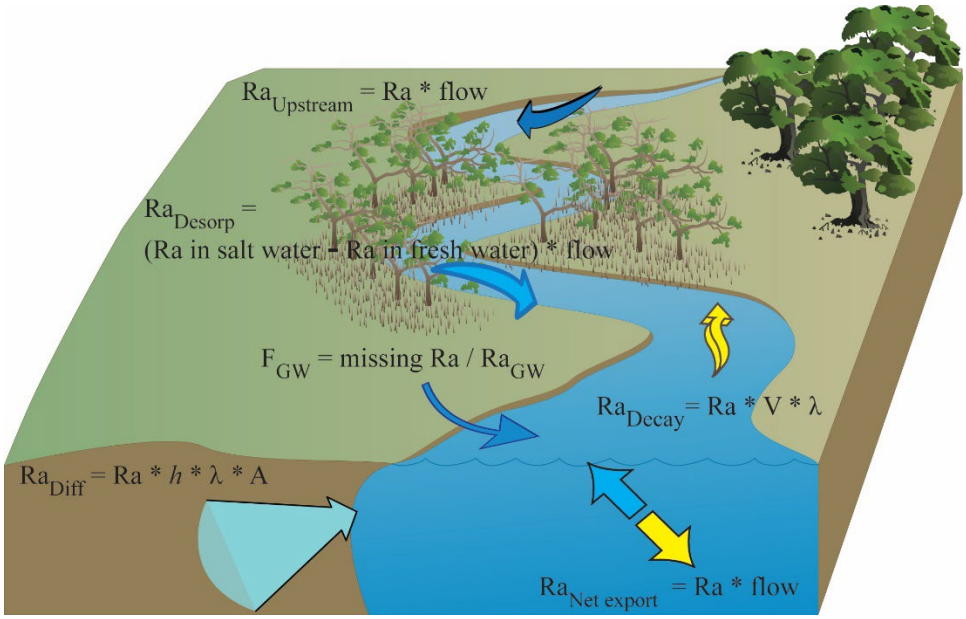

654

655

Figure 3. Time series measurements of surface water radium and ancillary data at all sites. Closed circles represent measurements taken at top of the water column while open circles indicate measurements at the bottom.

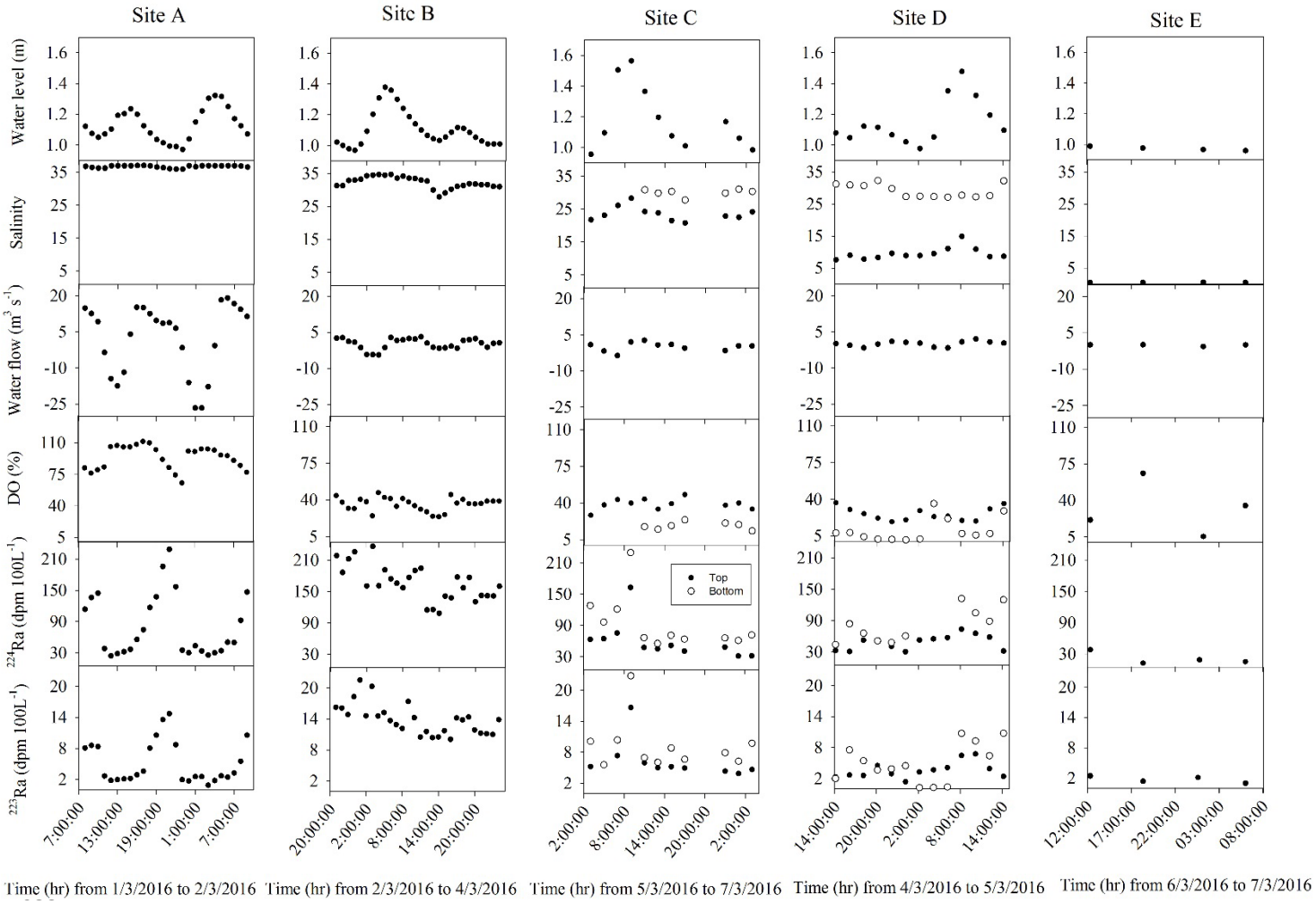

Figure 4. Water column measurements of salinity, dissolved oxygen (DO; % saturation) and temperature (˚C) at each station which are represented by the black dots.

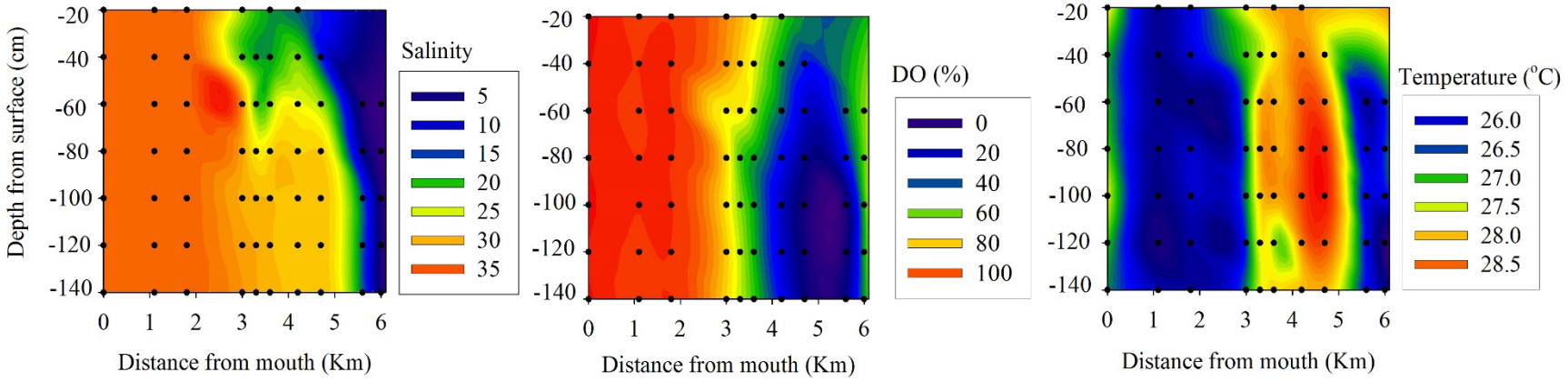

Figure 5. Salinity, DO, radium concentration and residence time maps for top and bottom layer of Coffs Creek estuary. Radium-224 show similar trends to ^{223}Ra.

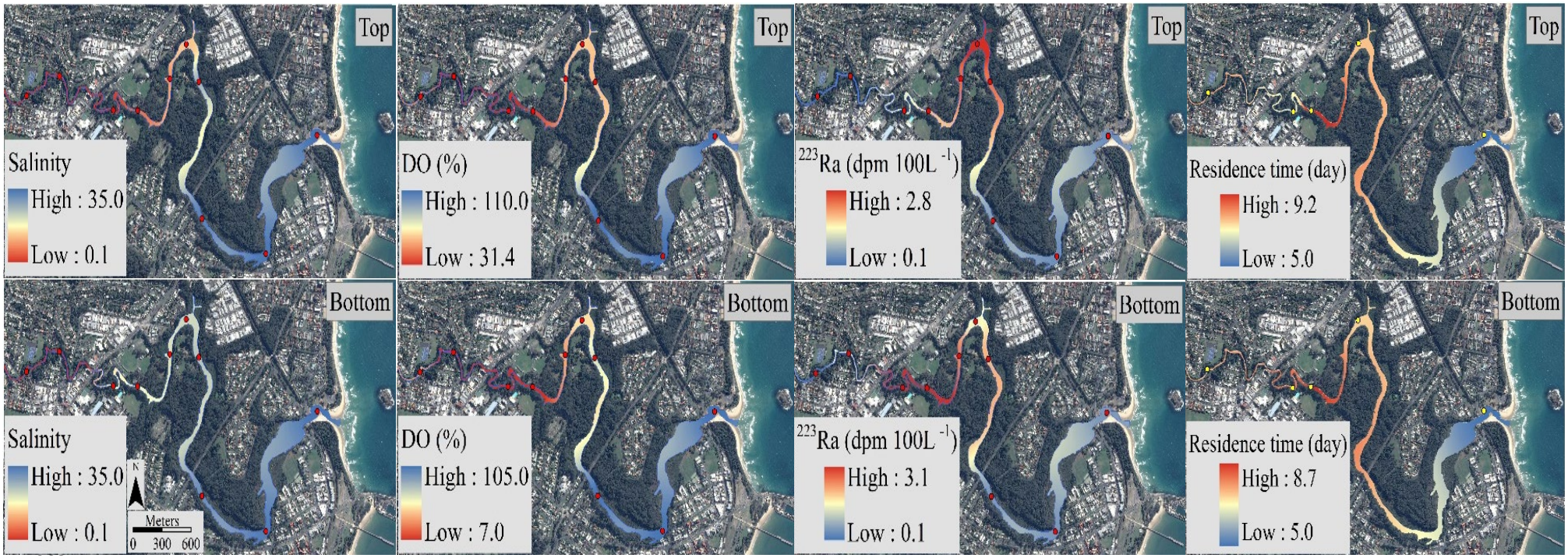

674 Figure 6. Porewater exchange rates from ^{223}Ra and ^{224}Ra along different section of the estuary
675 with and without mangrove vegetation and ratio of mangrove area to estuary area in each section.

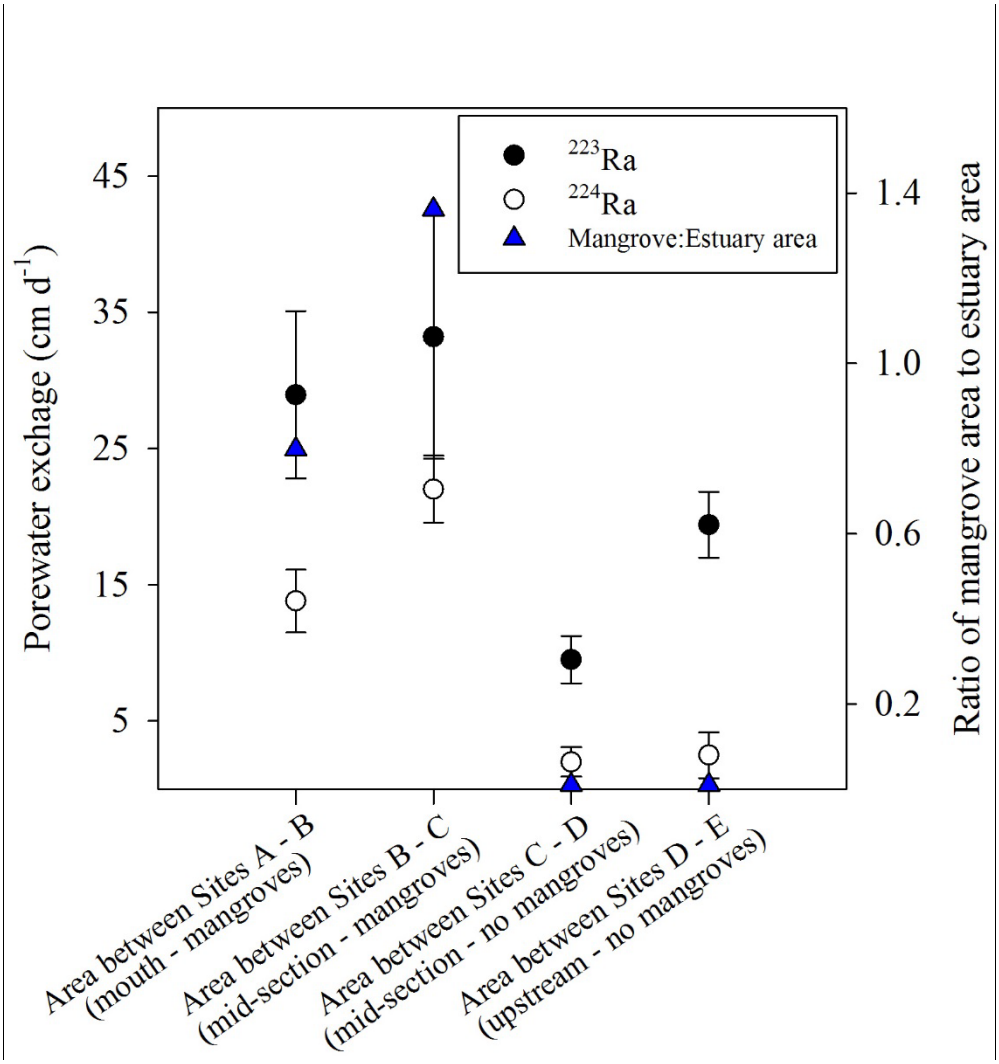

676

677

678 Figure 7. Radium versus salinity scatter plots for surface water and groundwater. Notice the scale
679 break.

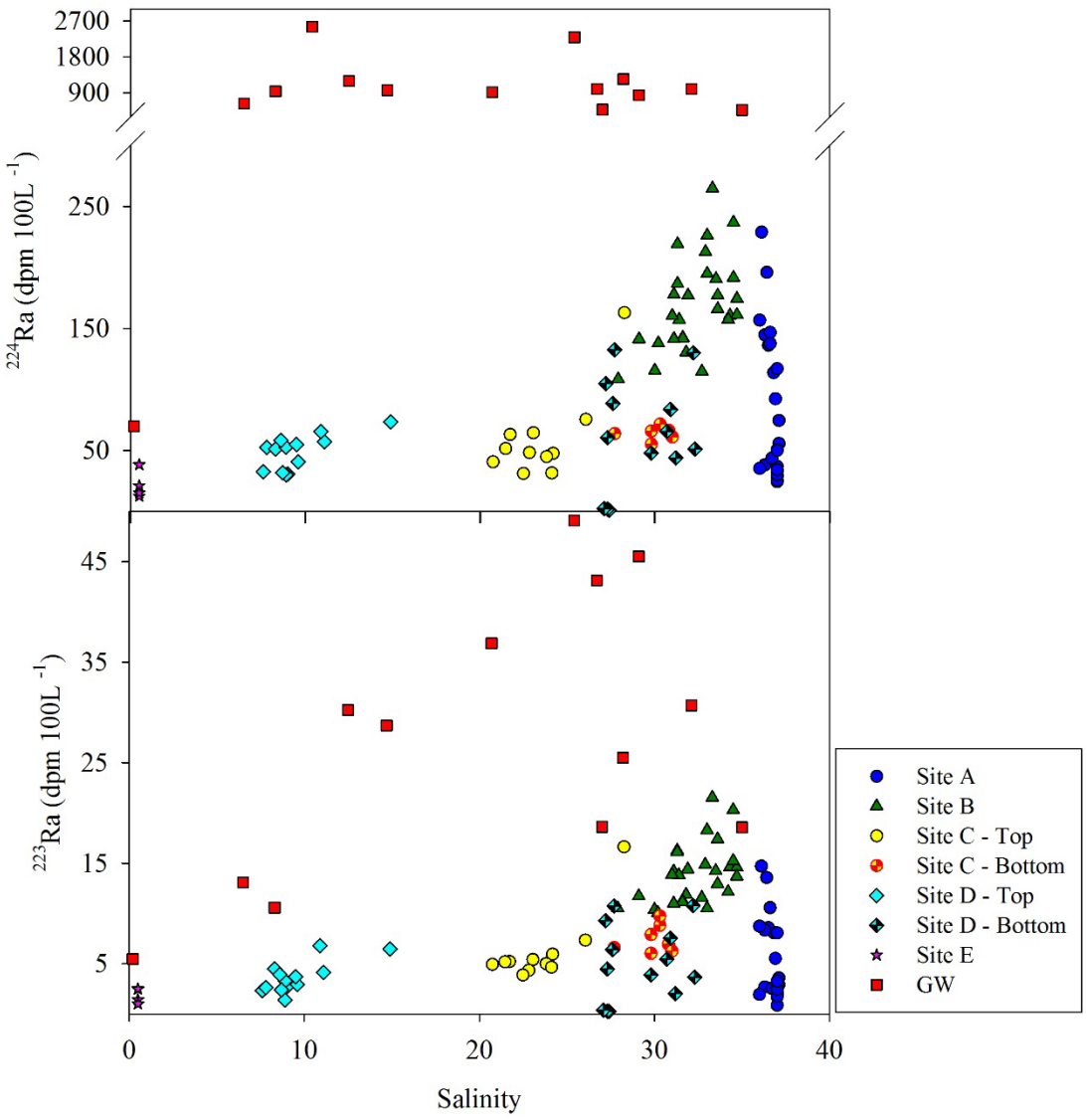

680

681

682

683 Figure 8. The ratio of ^{223}Ra to ^{224}Ra concentrations for surface and groundwater.

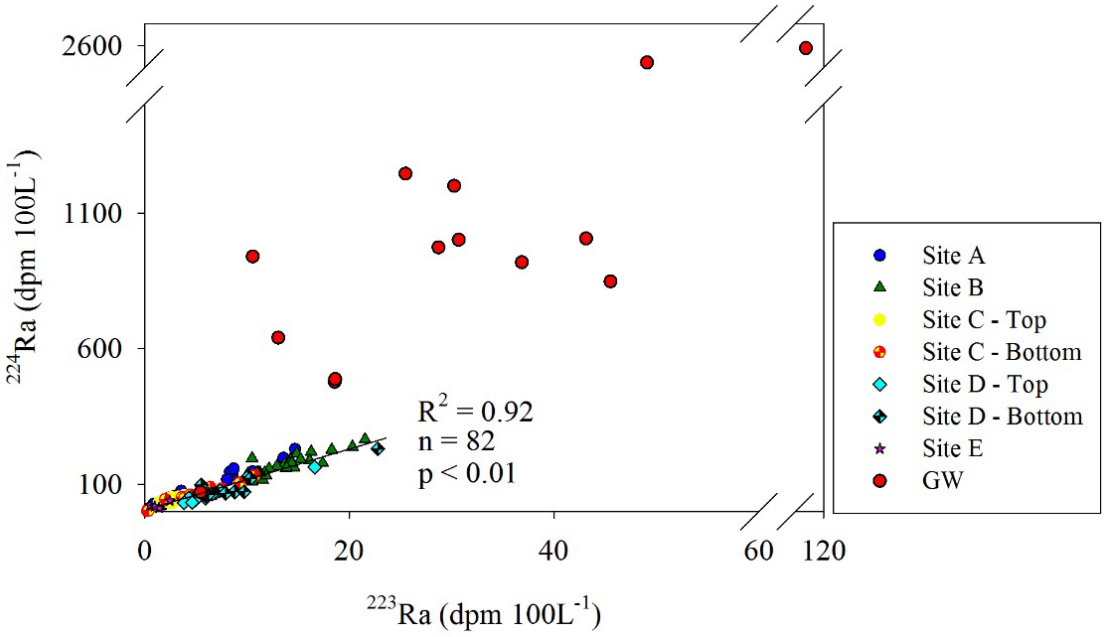

684

685 Figure 9. Hysteresis patterns in surface water ^{223}Ra and ^{224}Ra concentrations versus water depth
686 for Site A.

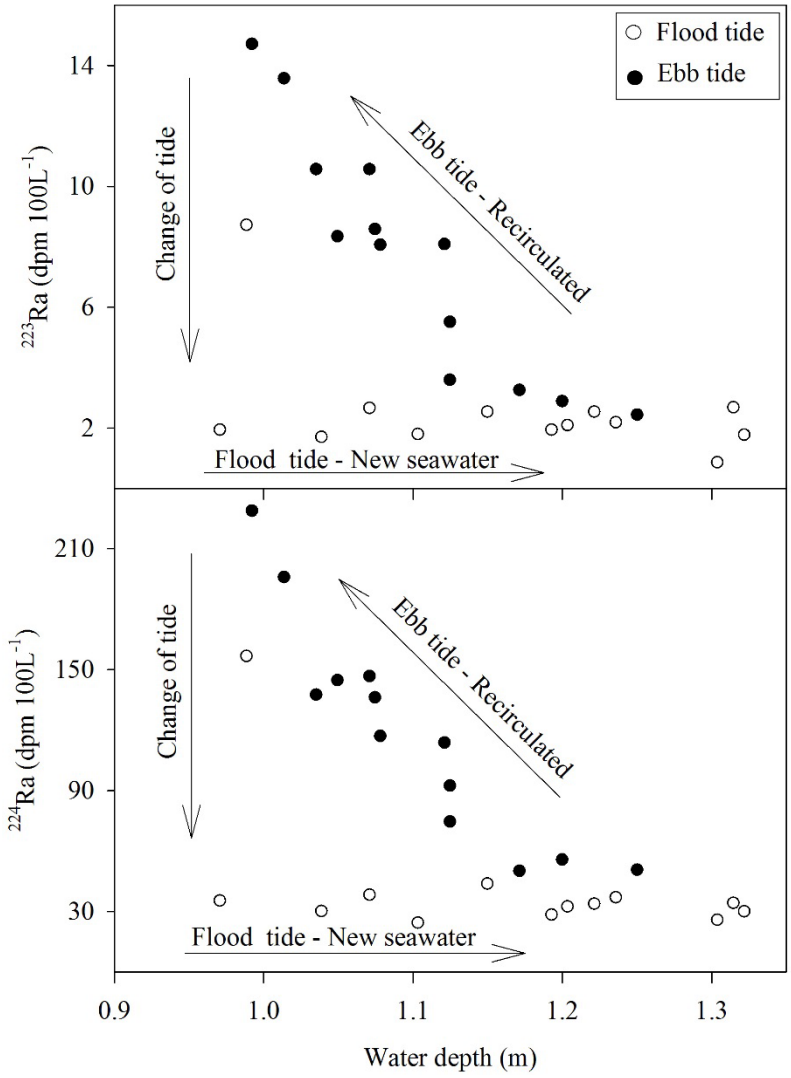

687

688

689 Figure 10. Salinity and short-lived radium isotopes versus dissolved oxygen saturation in surface water and groundwater.

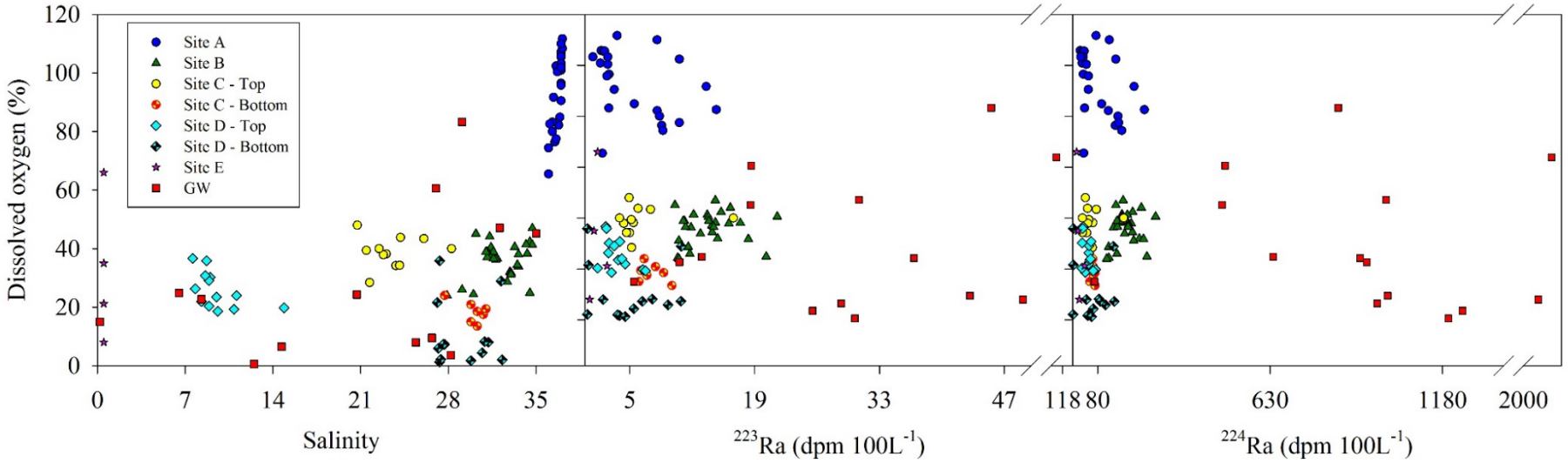

690

691

692 Table 1. Radium concentrations and physiochemical parameters of groundwater in the Coffs Creek estuary.

Sample	Coordinates	Salinity	DO (%)	Temp. (°C)	Depth (m)	^{223}Ra (dpm 100L^{-1})	^{224}Ra (dpm 100L^{-1})
1	S30 17.661 E153 07.099	14.7	6.5	23.3	0.4	28.7±3.1	972±24
2	S30 17.672 E153 07.096	20.7	24.3	22.5	0.5	36.8±3.7	917.4±23.2
3	S30 17.681 E153 07.077	12.5	0.6	24.2	2.0	30.2±3.3	1199.1±28.7
4	S30 17.668 E153 07.085	10.4	63.9	24.0	3.0	113.8±6.9	2557.3±38.8
5	S30 17.764 E153 08.210	29.1	83.3	29.1	0.3	45.5±6.1	847.2±33.4
6	S30 17.763 E153.08220	35.0	45.2	28.5	0.4	18.5±3.9	476.6±27.4
7	S30 17.763 E153 08.215	32.1	47.1	29.1	0.5	30.7±4.9	1000.3±40.1
8	S30 17.768 E153.08217	26.7	9.5	27.3	0.3	43.1±6.3	1005.3±39.9
9	S30 17.666 E153 07.251	8.3	22.7	23.1	2.3	10.5±1.8	938.7±28.7
10	S30 17.669 E153 07.251	6.5	24.8	24.4	3.0	13.1±2.5	639.8±26.1
11	S30 17.835 E153 07.441	0.2	15.0	22.4	28.0	5.4±1.9	69.8±7.1
12	S30 17.516 E153.07445	27.0	60.6	24	1.5	18.6±3.6	486.7±24.1
13	S30 17.509 E153.07.430	28.2	3.6	24.3	1.5	25.5±6.1	1244.3±71.8
14	S30 17.512 E153.07.434	25.4	8.0	25.4	1.2	49.1±8.1	2297.1±91.1
Average		19.8	29.7	25.14	3.21	33.5	1046.6
STD Error		2.9	6.7	0.64	1.92	7.1	177.6

693

694

695 Table 2. Radium mass balance terms and radium-derived porewater exchange rates for Coffs Creek estuary.

		^{223}Ra									
	Units	Area between Site A - B	Unc.	Area between Site B - C	Unc.	Area between Site C - D	Unc.	Area between Site D - E	Unc.	Total	Unc.
Upstream inputs	dpm s^{-1}	30.28	4.03	8.61	1.04	4.86	0.68	1.47	0.33		
Diffusion	dpm s^{-1}	1.98	0.59	0.19	0.06	0.15	0.04	0.05	0.01		
Ra decay	dpm s^{-1}	0.70	0.40	0.29	0.10	0.08	0.05	0.02	0.01		
Desorption	dpm s^{-1}	0	0	0	0	0	0	0.32	0.03		
Downstream outputs	dpm s^{-1}	251.25	37.25	30.28	4.03	8.61	1.04	4.86	0.68		
Missing (porewater)	dpm s^{-1}	225.85	37.58	23.84	4.04	3.69	0.36	3.39	0.35		
Porewater exchange	m^3 s^{-1}	0.7	0.1	0.06	0.01	0.01	0.002	0.01	0.001	0.8	0.1
Porewater exchange	cm d^{-1}	28.0	6.1	31.3	5.9	9.5	1.6	20.4	3.3	27.8	5.3
		^{224}Ra									
Upstream inputs	dpm s^{-1}	548.56	55.99	56.96	5.83	30.74	4.57	16.77	0.67		
Diffusion	dpm s^{-1}	65.37	19.61	11.39	3.42	9.64	2.89	2.67	0.80		
Ra decay	dpm s^{-1}	24.34	14.30	11.38	5.60	3.29	1.75	1.01	0.52		
Desorption	dpm s^{-1}	0	0	0	0	0	0	1.25	0.12		
Downstream outputs	dpm s^{-1}	3886.60	549.23	548.56	55.99	56.96	5.83	30.74	4.57		
Missing (porewater)	dpm s^{-1}	3377.78	552.70	492.29	52.46	24.04	0.54	13.55	3.73		
Porewater exchange	m^3 s^{-1}	0.3	0.1	0.05	0.01	0.002	0.001	0.001	0.001	0.4	0.1
Porewater exchange	cm d^{-1}	13.5	2.3	22.0	2.5	1.6	0.1	2.5	0.7	13.6	2.1

696